PERGAMON

International Journal of Heat and Mass Transfer 41 (1998) 4341–4349

International Journal of HEAT and MASS TRANSFER

Two-phase flow patterns and transition characteristics for in-tube condensation with different surface inclinations

W. C. Wang*, X. H. Ma, Z. D. Wei, P. Yu

Thermal Engineering Department, Tsinghua University, Beijing 100084, People's Republic of China

Received 25 September 1996; in final form 10 January 1998

Abstract

In-tube condensation of R-11 was experimentally investigated with various surface inclination angle between the direction of the vapor flow and the gravitational force, φ. The two-phase flow patterns were observed visually and the transition locations between different flow patterns were measured in a transparent test section. The vapor quality distribution along the test tube and the measured transition locations were used to prepare a flow pattern map. The experimental results indicated that the surface inclination, φ, strongly influenced the vapor and condensate distribution. Annular flow spanned the whole tube for $\varphi = 0^\circ$ at various vapor flow rates. Annular flow and stratified flow patterns were observed for $\varphi = 45^\circ$ and 60°. Annular flow, stratified flow, half-slug flow, and slug flow exist in sequence for $\varphi = 90$–120°. Annular flow, churn flow and slug flow occurred for $\varphi = 180^\circ$. The possible prediction of flow patterns for in-tube condensation in a microgravity environment was discussed briefly.

Nomenclature

A tube inside cross-sectional area [m^2]
c_p specific heat [J kg^{-1} K^{-1}]
C empirical parameter in equation (8)
D tube diameter [m]
G mass velocity [kg s^{-1} m^{-2}]
h_{fg} latent heat of condensation [kJ kg^{-1}]
j superficial velocity [m s^{-1}]
m mass flow rate [kg s^{-1}]
n empirical parameter in equation (8)
Q heat transfer rate [W]
t temperature [°C]
We Weber number
x vapor quality.

Greek symbols
ρ density [kg m^{-3}]
σ surface tension [N m^{-1}]
φ surface inclination [°].

Subscripts
g vapor phase
G vapor phase
i ith sub-section of Section A
in tube inlet
l liquid phase
L liquid phase
out tube outlet
R refrigerant
S saturation
w cooling water.

1. Introduction

Flow condensation in tube has various practical applications, such as in the chemical process industry, in refrigeration and air-conditioning systems, etc. The two-phase flow patterns along the tube significantly affect the local heat transfer coefficient. Therefore, many investigations of the flow patterns for in-tube condensation have been reported in literatures. The gravitational force and the vapor–liquid interfacial shear stress are known as two dominant factors controlling the vapor and liquid distribution inside the tube and, hence, the various flow patterns along the tube, and hence, the previous investigations were mostly concerned with the two-phase flow

* Corresponding author.

0017–9310/98 $19.00
PII: S0017–9310(98)00041–6

pattern for condensation in horizontal tubes [1–5]. These studies had successfully provided informations about the types of flow patterns existing along the condensation path, as well as experimental data specifying the flow conditions under which each pattern is expected to exist. Carey [6] gave a more detailed review of flow patterns for in-tube condensation.

Recent demands for compact and high performance condensers in aerospace thermal control technology with capillary pumped loop systems have stimulated interest in in-tube condensation heat transfer in microgravity. So far, experimental studies have been published concerning the flow patterns of adiabatic water–air two-phase flow in a tube under microgravity conditions [7–8]. However, few reports were found in the literature describing the flow patterns for in-tube condensation under microgravity conditions [9].

The objective of the present investigation is to obtain information about how the gravitational force affects the two-phase flow pattern for condensation in a small diameter tube. The flow pattern map and the transition conditions for the different flow patterns were determined from the experimental results. In addition, the condensation flow patterns under microgravity condition were deduced from the results of this investigation and those of ref. [10].

2. Experimental facilities

Figure 1 shows the schematic diagram of the experimental apparatus used for in-tube condensation of R-11. The apparatus includes the test section, refrigerant system and cooling water system.

The test sections, A and B, are fixed onto a platform which could be easily rotated around an axis to change the surface inclination. The refrigerant flowed inside the tube with parallel flow of water in the annulus. Section A, which was made of a 6 mm I.D. copper tube and a 16 mm I.D. Plexiglas annulus, was divided into six subsections to measure the local heat transfer performance. Each sub-section was 200 mm long. Three thermocouples are installed on the outside wall of the copper tube at different locations to determine the mean wall temperature. The transparent part, Section B, allowed visual investigation of the flow pattern for condensation of R-11 along the test tube. A 1200 mm long and 6 mm I.D. quartz glass tube used as the test tube was surrounded by a 15 mm $\times$ 15 mm cross-section rectangular annulus with parallel flow of the cooling water.

The refrigerant vapor was first evaporated in a refrigerant tank with an immersion heater, and then flowed through a preheater and condensed in the tube cooled by the water flowing in the annulus. The vapor entering the test section was kept slightly superheated by an electric preheater wrapped around the tube. The preheater was controlled by a voltage regulator. The refrigerant mass flow rate was measured with the special apparatus shown in Fig. 2. The refrigerant mass flow rate could be calculated from the input electric power and the inlet and outlet temperatures of the refrigerant flowing in the annulus.

The cooling water from an elevated tank entered the annulus around the test section at a specified temperature and flow rate. The water inlet temperature was controlled by a 2 kW heater immersed in the water tank. The water flow rate was controlled by a valve and measured by weighing the water flow. The water inlet and outlet temperatures for every sub-section of test section A were measured by copper–constantan thermocouples which were inserted into a mixer. The mixer was used to maintain a uniform cooling water temperature. All thermocouples were calibrated in the same constant-temperature bath with an accuracy of $\pm 0.1^{\circ}$C.

3. Data reduction

The condensation flow patterns for R-11 in the test tube were investigated visually in section B to measure the transition locations between the different flow patterns. Then, the vapor quality distribution along the test tube was determined in section A. The complete flow pattern map and the transition conditions were, therefore, determined for the different flow patterns. All data was collected with a HP3852A data acquisition/control unit and reduced with a personal computer.

The heat transferred through the cooling water was calculated by:

$$Q_{\mathrm{w}} = c_{\mathrm{pw}} m_{\mathrm{w}} (t_{\mathrm{w},7} - t_{\mathrm{w},1}) \tag{1}$$

where $t_{\mathrm{w},7}$ and $t_{\mathrm{w},1}$ denote the outlet and inlet temperatures of the cooling water in Section A, respectively.

The condensation heat flux was determined by:

$$Q_{\mathrm{R}} = m_{\mathrm{R}} \cdot h_{\mathrm{fg}} \tag{2}$$

where m_{R} is the refrigerant mass flow rate measured in the special measuring apparatus.

The heat balance for the apparatus was checked by comparing the two heat fluxes, which agreed within 10% for every experiment. It was conservatively estimated that the experimental uncertainties in the vapor mass flow rate and the condensation heat flux were 2 and 8%. Details of the error analysis have been reported in ref. [11].

Assuming that the vapor quality varied linearly within each sub-section and between sub-sections, the inlet and exit vapor qualities for every sub-section in test Section A were determined by:

$$x_{i+1} = x_i - \frac{Q_i}{Q_{\mathrm{w}}} \tag{3}$$

$$Q_i = m_{\mathrm{w}} \cdot c_{\mathrm{pw}} (t_{\mathrm{out},i} - t_{\mathrm{in},i}), \quad i = 1 \sim 6 \tag{4}$$

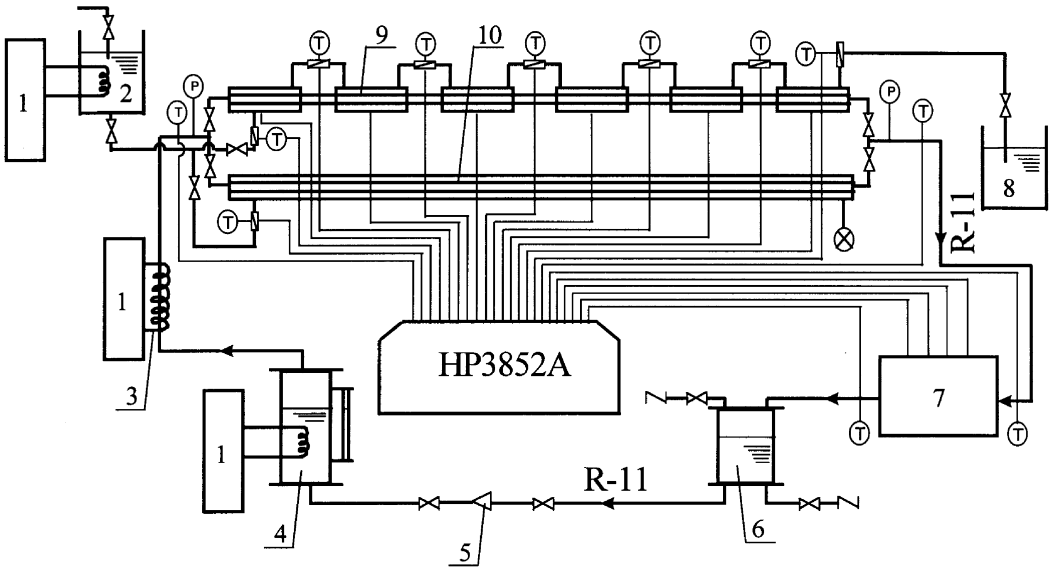

1-Voltage Regulator ; **2**-Water Tank; **3**-Pre-heater; **4**-Evaporator; **5**-Pump;
6-Refrigerant Tank; **7**-Measuring Apparatus for Refrigerant Mass Flow Rate
8-Weighing Water Tank; **9**-Section A; **10**-Section B

Fig. 1. Experimental apparatus.

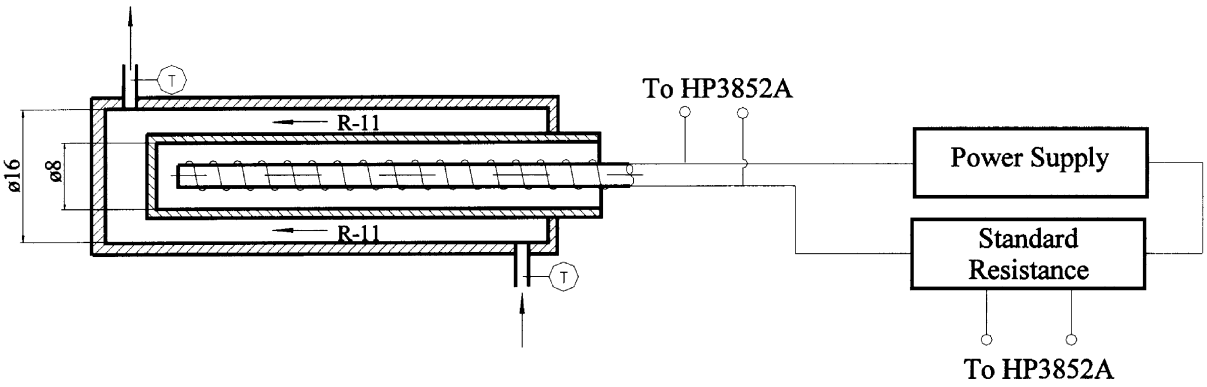

Fig. 2. Measuring apparatus for refrigerant mass flow rate.

where subscripts 'out' and 'in' denote that referred to the inlet and exit of tube, respectively.

The refrigerant mass velocity in the tube is:

$$GR = \frac{m_R}{A} \tag{5}$$

The superficial liquid velocity and the superficial vapor velocity are:

$$j_L = G_R \cdot (1-x)/\rho_l \quad \text{and} \quad j_G = G_R \cdot x/\rho_g. \tag{6}$$

The corresponding Weber numbers are defined, respectively, as:

$$We_{S,L} = j_l^2 D\rho_l/\sigma \quad \text{and} \quad We_{S,G} = j_G^2 D\rho_g/\sigma. \tag{7}$$

The flow pattern map and the transition conditions between flow patterns were correlated with the Weber number.

4. Results and discussion

4.1. Flow patterns and transition locations

Figures 3 and 4 show the schematic drawings and the corresponding photographs of the flow patterns for in-

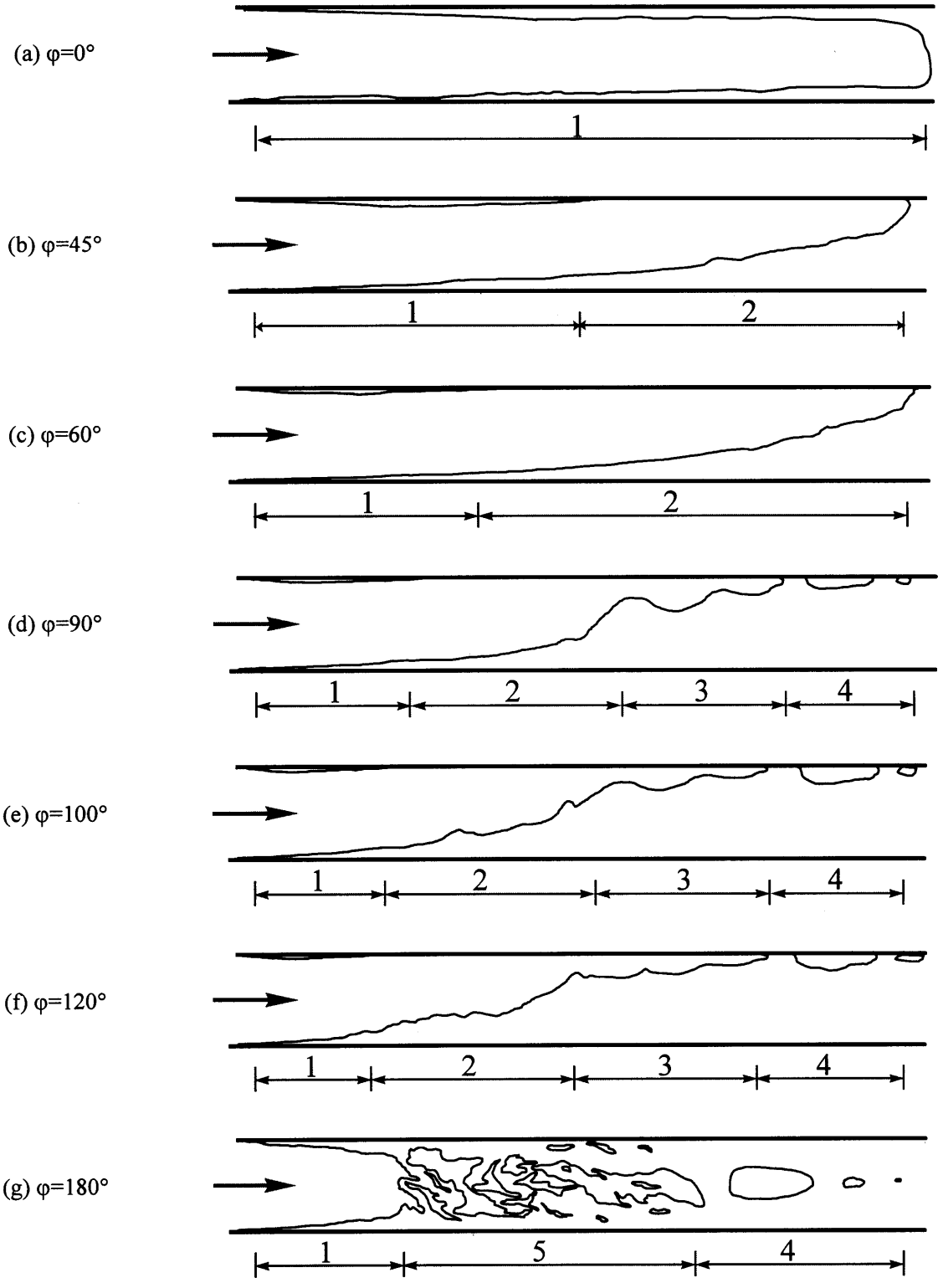

Fig. 3. Schematic drawings of condensation flow patterns for various φ.

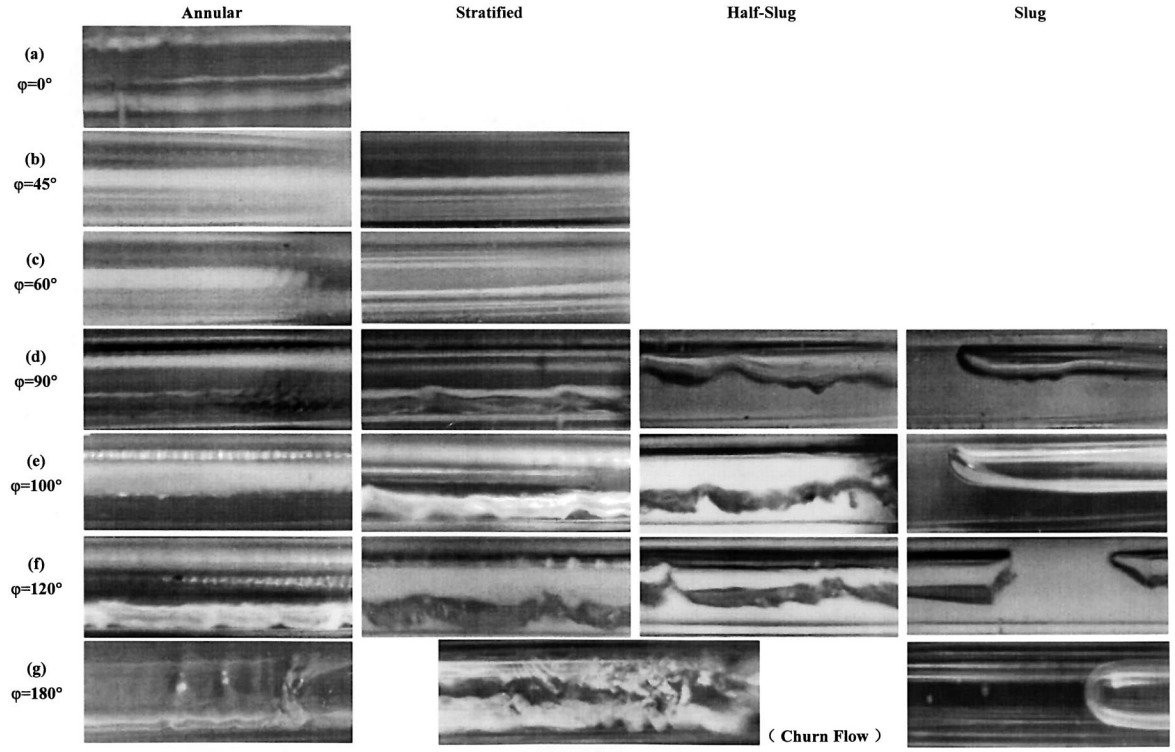

Fig. 4. Photographs of condensation flow patterns for various φ.

tube condensation of R-11 at different surface inclinations. Here, the vapor flow direction entering the test tube was defined as the positive direction and the surface inclination angle is between the gravitational force and the vapor flow direction. For a vertically orientated test tube and downward vapor flow, i.e. $\varphi = 0^\circ$, both the gravitational force and the vapor shear force caused the condensate to drain downward along the wall while the vapor flowed in the core of the tube, and annular flow spanned the entire condensation path as shown in Fig. 3(a) and Fig. 4(a). For $\varphi = 45^\circ$, the condensate was stratified within the tube by the portion of the gravitational force perpendicular to the wall. Consequently, annular flow and stratified flow patterns occurred in the test tube, Fig. 3(b) and Fig. 4(b). Similar results were obtained with a surface inclination of 60°, Fig. 3(c) and Fig. 4(c).

When the refrigerant condensed in a horizontal tube, i.e. $\varphi = 90^\circ$, annular flow, stratified flow, half-slug flow and slug flow patterns were observed within the tube as shown in Fig. 3(d) and Fig. 4(d). The liquid–vapor interfacial shear force thickened the condensate film in the stratified flow region, causing a wavy interface with intermittent half slug and slug flow patterns. Because the decrease in vapor quality along the test tube caused the condensate mass flow rate to increase, bubbles within the slug flow regime existing along the top portion of the tube quickly collapsed due to vapor condensation. Single-phase liquid flow occurred at the tube exit. For surface inclinations of 100 and 120°, the flow patterns were very similar to those for $\varphi = 90^\circ$, Fig. 3(e)–(f) and Fig. 4(e)–(f) except that the vapor–liquid interface became more turbulent at larger inclinations.

For $\varphi = 180^\circ$ with upward vapor flow, annular flow, churn flow and slug flow patterns were observed separately along the condensation path. The gravitational force acting counter to the vapor flow caused violent interaction of the vapor and liquid making it very difficult to identify stratified flow and half-slug flow patterns within the tube. Therefore, the flow was characterized as churn flow. Near the exit, slug flow was observed due to the condensation along the test tube.

The annular flow was observed at the tube inlet for all the cases studied here. The inlet vapor flow rate and the degree of surface subcooling may be the dominant factors controlling the vapor–liquid geometry at the beginning of the condensation path. This differs from that reported in [12], for which moist flow was normally observed at the tube inlet. In addition, bubbly flow was not observed in the present experiments. The vapor flow rate became quite low due to continuous condensation along the test tube, so that the vapor–liquid interfacial stress force was

not adequate to collapse the large slug bubble into small bubbles as to form bubbly flow.

The flow pattern transition locations, which were defined as the distance between the tube inlet and the point where the specified flow pattern occurred, are presented in Tables 1–3. L_1, L_2 and L_3 in Tables 1 and 2 denote the transition locations from annular flow to stratified flow, from stratified flow to half-slug flow and from half-slug flow to slug flow. L_4 and L_5 in Table 3 indicate the transition locations from annular flow to churn flow and from churn flow to slug flow. The transition locations between different flow patterns were found to occur earlier in the tube as the vapor flow rate increased.

4.2. Flow pattern map and correlation of transition characteristics

Figure 5 illustrates the flow pattern maps for all cases investigated here. The Weber number for the vapor was chosen relative to the vertical direction while the Weber number for the liquid was chosen relative to the horizontal direction so that the transition conditions between different flow patterns can be correlated as follows:

$$We_{S,G} = C \cdot We_{S,L}^{n}. \quad (8)$$

Table 4 presents the values of C and n for the various surface inclinations as determined from the experimental data for the transitions between the different flow patterns. The parameters C and n were then correlated as a function of surface inclination and flow pattern.

For $\varphi \leqslant 90^\circ$, the transition from annular flow to stratified flow were correlated as:

$$C = 97.1(1-\cos\varphi)^{0.153} \quad (9)$$

$$n = 0.459\, e^{0.183(1-\cos\varphi)} \quad (10)$$

For $90^\circ \leqslant \varphi < 180^\circ$, the transitions between different flow patterns were correlated as:

(1) Transition from annular flow to stratified flow:

$$C = 187.2 - 247.9(1-\cos\varphi) + 145.3(1-\cos\varphi)^2 \quad (11)$$

Table 1
Transition locations from annular to stratified flow for $\varphi = 45$ and 60°

$\varphi = 45^\circ$		$\varphi = 60^\circ$	
m_R [kg s^{-1} m^{-2}]	L_1 [cm]	m_R [kg s^{-1} m^{-2}]	L_1 [cm]
14.0	10	13.2	9
22.5	18	21.4	17
31.8	27	30.2	28
42.1	30	40.0	34
44.0	30	42.1	27
72.7	40	68.5	38
75.5	41	71.5	39
123.2	54	120.1	52

Table 3
Transition locations between different flow patterns for $\varphi = 180^\circ$

m_R [kg s^{-1} m^{-2}]	L_4 [cm]	L_5 [cm]
9.0	4	55
14.6	6	65
18.8	8	70
25.4	12	79
26.3	12	72
42.9	16	80
45.2	16	85
63.1	20	91

Table 2
Transition locations between different flow patterns for $\varphi = 90$, 100 and 120°

$\varphi = 90^\circ$				$\varphi = 100^\circ$				$\varphi = 120^\circ$			
m_R [kg s^{-1} m^{-2}]	L_1 [cm]	L_2 [cm]	L_3 [cm]	m_R [kg s^{-1} m^{-2}]	L_1 [cm]	L_2 [cm]	L_3 [cm]	m_R [kg s^{-1} m^{-2}]	L_1 [cm]	L_2 [cm]	L_3 [cm]
11.3	25	70	93	9.9	19	36	85	9.5	9	24	82
17.9	30	75	97	15.9	25	44	90	15.4	13	33	87
24.4	32	77	100	20.7	25	39	96	20.0	16	29	90
31.4	36	80	104	28.3	30	47	99	27.2	21	39	94
32.1	35	79	101	29.8	30	51	95	27.9	18	41	92
53.7	40	82	104	46.1	35	58	99	44.1	25	51	96
55.9	40	83	106	48.5	35	55	102	46.8	26	47	96
81.7	44	85	108	67.8	40	62	105	65.4	30	56	98

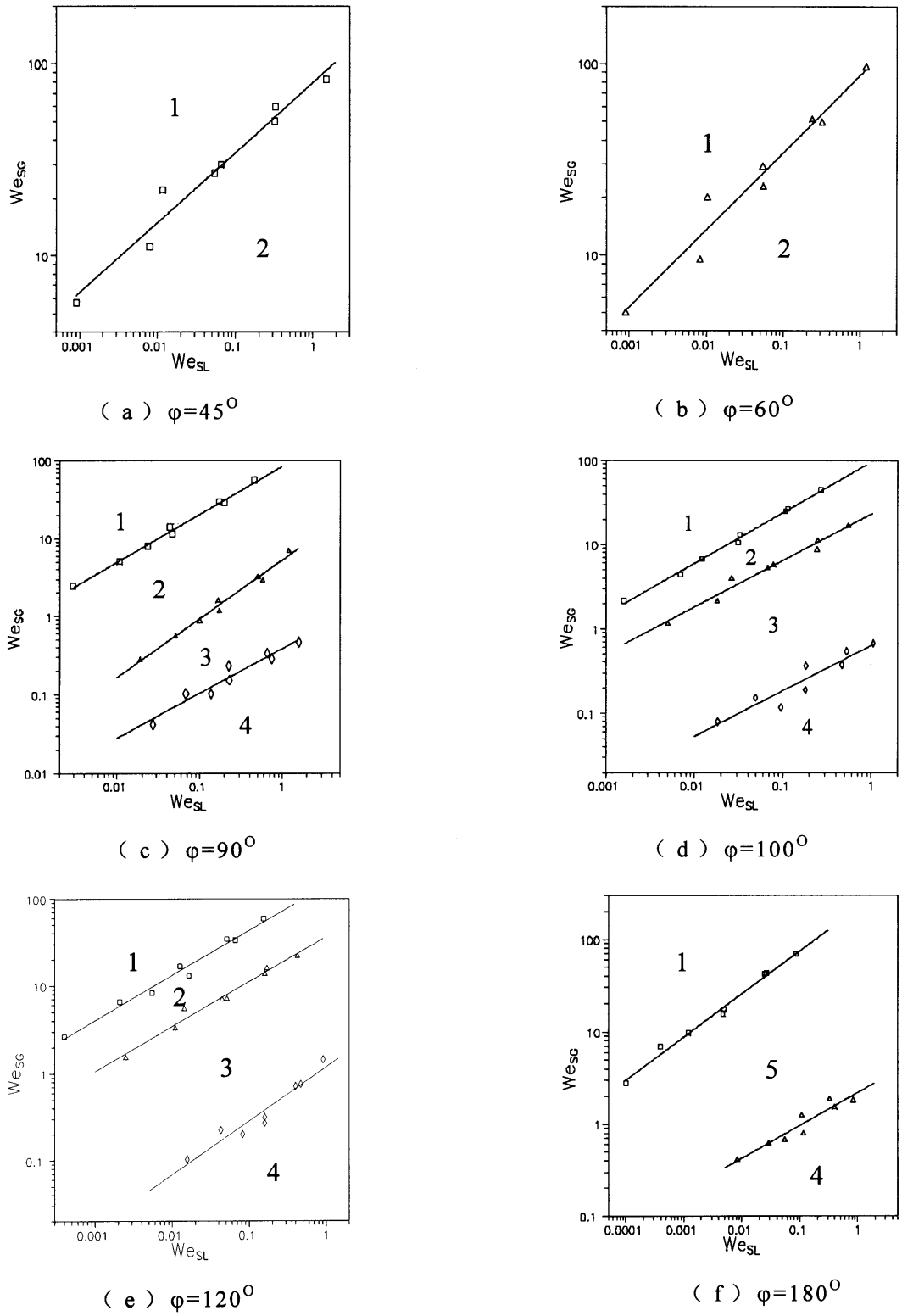

Fig. 5. Flow pattern maps for in-tube condensation for various φ.

Table 4
Values of the empirical parameters C and n in equation (8)

φ	Annular to stratified	Stratified to half-slug	Half-slug to slug
0°	—	—	—
45°	$C = 80$, $n = 0.364$	—	—
60°	$C = 87.3$, $n = 0.404$	—	—
90°	$C = 84.6$, $n = 0.615$	$C = 5.70$, $n = 0.752$	$C = 0.388$, $n = 0.57$
100°	$C = 96.4$, $n = 0.603$	$C = 23.2$, $n = 0.553$	$C = 0.635$, $n = 0.536$
120°	$C = 142.3$, $n = 0.516$	$C = 36.4$, $n = 0.512$	$C = 1.19$, $n = 0.619$
	Annular to churn	Churn to slug	
180°	$C = 219.0$, $n = 0.465$	$C = 2.21$, $n = 0.358$	

$$n = 0.221 + 0.789(1-\cos\varphi) - 0.3948(1-\cos\varphi)^2. \quad (12)$$

(2) Transition from stratified flow to half-slug flow:

$$C = -236.8 + 363.2(1-\cos\varphi) - 120.7(1-\cos\varphi)^2 \quad (13)$$

$$n = 4.294 - 5.584(1-\cos\varphi) + 2.04(1-\cos\varphi)^2. \quad (14)$$

(3) Transition from half-slug flow to slug flow:

$$C = -0.405 + 2.056(1-\cos\varphi) - 0.537(1-\cos\varphi)^2 \quad (15)$$

$$n = 1.822 - 2.153(1-\cos\varphi) + 0.9(1-\cos\varphi)^2. \quad (16)$$

4.3. On the prediction of flow patterns for in-tube condensation under microgravity conditions

An understanding of the flow patterns for condensation under microgravity conditions is very important in a variety of space applications. As reported in [10], the flow patterns for adiabatic water–air flow in microgravity are very similar to those in normal gravity with upward flowing air, but churn flow occurs only in normal gravity. Comparison between flow patterns for adiabatic upward flow of water–air flow and the in-tube condensation in normal gravity reveals that, these two-phase systems have very similar flow patterns except that bubble flow and wispy-annular flow are not observed during condensation. Hence, the flow patterns for in-tube condensation in microgravity can be deduced from both adiabatic two-phase water–air flow in microgravity and in-tube condensation in normal gravity conditions.

It is well known that, the vapor condenses and forms a condensate film on the cooled wall, both in microgravity and normal gravity. The flow characteristics for vapor and liquid within a tube should be identical for condensate flow and for adiabatic two-phase water–air flow since the driving forces acting at the liquid film interface would be the same for both cases in microgravity, the surface tension will be dominant in the case under microgravity, especially when the vapor flow rate is small.

It makes clear that, in microgravity, the two-phase flow patterns for in-tube condensation should include annular flow and slug flow, and bubbly flow and wispy-annular flow will not occur.

Churn flow was observed in normal gravity when the gravitational force was comparable to the vapor inertial force. Annular-slug flow will occur in microgravity when the vapor inertial force is comparable to the surface tension. The condensate film interface within this flow region would become wavy as the vapor flow rate increased and the film thickness decreased.

The transition locations between different flow patterns can be deduced by comparing the present results for upward vapor flow with the water–air flow pattern transitions in microgravity reported by Zhao and Rezkallah [10]. The condition for slug flow, $We_{s,G} < 1.0$, was consistent with the results of ref. [10] within the surface tension dominant region. For annular flow, present results are unlikely to predict the transition from annular flow to any other flow pattern in microgravity because the transitions reported here are strongly dependent upon the liquid flow rate, owing to the gravitational force acting on the liquid film. However, the transition condition provided by Zhao and Rezkallah [10] could be applied to predict the occurrence of annular flow, annular flow would be the possible flow pattern only for $We_{s,G} \geqslant 20.0$. Annular flow, slug flow and annular-slug flow, etc would occur for $1.0 < We_{s,G} < 20.0$.

5. Conclusions

Visualization experiments were conducted to determine the flow patterns for in-tube condensation of R-11 at various surface inclinations. The following conclusions can be drawn from the results.

(1) The surface inclination or the gravitational force has a significant impact on the flow patterns for in-tube condensation. The experimental observations also indicated that the flow patterns for in-tube condensation were significantly different from those for

adiabatic two-phase water–air flow and for flow boiling.

(2) For all the cases studied here, annular flow was commonly observed at the test tube entrance, while bubbly flow did not occur at the tube exit.

(3) Transition locations between different flow patterns moved up the tube with increasing vapor flow rate. The transition conditions can be correlated using: $We_{S,G} = C \cdot We_{S,L}^{n}$, with the values of C and n given in Table 4.

(4) The results of the present investigation and those of ref. [10] were used to predict the two-phase flow patterns for in-tube condensation in microgravity. The flow is expected to proceed from annular to annular-slug and slug flow along the condensation path. Transition conditions are proposed for the different flow patterns.

Acknowledgement

The project is currently supported by National Natural Science Foundation of China through contract 59586005.

References

[1] Rahman MM, Fathi AM, Soliman HM. Flow pattern boundaries during condensation: new experimental data. Canadian J Chem Eng 1985;63:547–52.

[2] Soliman HM, Azer NZ. Flow patterns during condensation inside a horizontal tube. ASHRAE Transactions 1971;77(1):210–24.

[3] Tandon TN, Varman HK, Gupta CP. A new flow regimes map for condensation inside horizontal tubes. ASME J Heat Transfer 1982;104:763–8.

[4] Traviss DP, Rohsenow WM. Flow regimes in horizontal two-phase flow with condensation. ASHRAE Transactions 1973;79(2):31–9.

[5] Soliman HM, Azer NZ. Visual studies of flow patterns during condensation inside horizontal tubes. In: Proc Fifth International Heat Transfer Conference, Tokyo 1974;3:241–5.

[6] Carey VP. Liquid–vapor phase-change phenomena. Washington, DC: Hemisphere Publishing, 1992.

[7] Dukler AE, Fabre JA, McQuillen JB, Vernon R. Gas–liquid flow at microgravity conditions: flow patterns and their transitions. Int J Multiphase Flow 1988;14:389–400.

[8] Colin C, Fabre JA, Dukler AE. Gas–liquid flow at microgravity conditions. Int J Multiphase Flow 1991;17:533–44.

[9] Keshock EG. A photographic study of flow condensation in 1-G and zero-gravity environments. In: Proc Fifth International Heat Transfer Conference, Tokyo 1974;3:236–40.

[10] Zhao L, Rezkallah KS. Gas–liquid flow patterns at microgravity conditions. Int J Multiphase Flow 1993;19:751–63.

[11] Wei ZD. Investigation of flow patterns and condensation heat transfer performance in-tube. M.S. thesis, Thermal Engineering Department, Tsinghua University, Beijing, 1997.

[12] Breber G, Palen JW, Teborek J. Prediction of horizontal tubeside condensation of pure components using flow regime criteria. ASME J Heat Transfer 1980;102:471–6.